# Space–Time Radial Basis Function–Based Meshless Approach for Solving Convection–Diffusion Equations

**Cheng-Yu Ku** [1,2,*] **, Jing-En Xiao** [2,*] **and Chih-Yu Liu** [1]

1   Department of Harbor and River Engineering, School of Engineering, National Taiwan Ocean University, Keelung 20224, Taiwan; 20452003@email.ntou.edu.tw
2   Center of Excellence for Ocean Engineering, National Taiwan Ocean University, Keelung 20224, Taiwan
*   Correspondence: 20452002@email.ntou.edu.tw (C.-Y.K.); chkst26@mail.ntou.edu.tw (J.-E.X.);
    Tel.: +886-2-2462-2192 (ext. 6109) (C.-Y.K.)

check for
updates

**Abstract:** This article proposes a space–time meshless approach based on the transient radial polynomial series function (TRPSF) for solving convection–diffusion equations. We adopted the TRPSF as the basis function for the spatial and temporal discretization of the convection–diffusion equation. The TRPSF is constructed in the space–time domain, which is a combination of $n$–dimensional Euclidean space and time into an $n + 1$–dimensional manifold. Because the initial and boundary conditions were applied on the space–time domain boundaries, we converted the transient problem into an inverse boundary value problem. Additionally, all partial derivatives of the proposed TRPSF are a series of continuous functions, which are nonsingular and smooth. Solutions were approximated by solving the system of simultaneous equations formulated from the boundary, source, and internal collocation points. Numerical examples including stationary and nonstationary convection–diffusion problems were employed. The numerical solutions revealed that the proposed space–time meshless approach may achieve more accurate numerical solutions than those obtained by using the conventional radial basis function (RBF) with the time-marching scheme. Furthermore, the numerical examples indicated that the TRPSF is more stable and accurate than other RBFs for solving the convection–diffusion equation.

**Keywords:** space–time; transient radial basis function; convection–diffusion equation; meshless; radial polynomials

## 1. Introduction

The convection–diffusion equation is extensively used in many contexts in scientific and engineering problems, such as those related to groundwater pollution [1], gas flow after-treatment systems [2], and methane reformation in catalytic reactors [3]. The convection–diffusion equation is a combination of diffusion and convection processes that are referred to as substance diffusion and concentration change, respectively. Numerical solutions for the convection–diffusion equation have been applied extensively by using conventional mesh–based approaches, such as the finite difference method (FDM) [4–6], finite volume method [7], finite element method (FEM) [8], and boundary element method (BEM) [9]. The Lattice Boltzmann method, which does not involve the use of a mesh, was adopted to simulate fluid flow in an elliptical honeycomb monolith reactor [10]. Greiner et al. applied X–ray microtomography to simulate the pore geometry and the distribution of the catalyst in the pores [11]. Li and Evans [12] adopted the BEM to solve heat convection–diffusion problems in homogeneous and isotropic media. Later, Sacco and Stynes [13] applied the Petrov–Galerkin FEM to solve the convection–diffusion equation. A global spectral analysis based on the finite difference scheme [14] was proposed to model the linear convection–diffusion equation in one

dimension. To increase the accuracy of results, optimal parameters are required for each proposed numerical scheme.

Unlike conventional mesh–based approaches, meshless approaches have gained attention because they do not require the tedious work of mesh construction or numerical integration. Among the meshless methods, the radial basis function (RBF) approach may be one of the simplest [15]. Over the last decade, research on meshless methods using RBFs to approximate partial differential equations (PDEs), such as the convection–diffusion equation, has accelerated. The multiquadric (MQ) RBF was proposed by Hardy [16] as an interpolation function for the analysis of gravitational fields. Subsequently, the Kansa method [17,18] that directly adopts the MQ RBF has been indicated to be an effective numerical tool for approximating PDE solutions. Numerous engineering problems, including Burgers' equation [19,20], heat transfer [21–23], and groundwater contaminant transport [24], have been solved using the Kansa method.

In the Kansa method, the optimal shape parameter must be determined. Attempts related to this topic have been conducted [25,26]. Tsai et al. [27] proposed the golden-section search algorithm to select the optimal shape parameter of the MQ RBF to solve PDEs. Ng et al. [28] utilized a new higher–order RBF–FD scheme with optimal variable shape parameters for solving a PDE. The optimum is computed by using the FDM combined with compact differencing schemes. Although MQ RBF in conjunction with the time-marching scheme [29–31] is an effective numerical tool for solving time-dependent PDEs, the time interval must be minimized to increase the result accuracy.

This study adopted the transient radial polynomial series function (TRPSF) as the basis function for spatial and temporal discretization. The TRPSF is based on the space–time domain, which is a combination of $n$–dimensional Euclidean space and time into an $n + 1$–dimensional manifold. Because both initial and boundary conditions are assigned in the space–time domain, we transformed an initial value problem to an inverse boundary value problem. Accordingly, the time–marching algorithm is not required in the presented approach. Several numerical implementations were conducted and compared with the Kansa method as well as other methods. The remainder of this paper is structured as follows. Section 2 introduces the mathematical formulation. To demonstrate the robustness and effectiveness of the proposed method, Section 3 presents the validation and convergence analysis. Section 4 presents numerical examples. Finally, concluding remarks are drawn in Section 5. The formulation of the proposed method is presented subsequently.

## 2. Mathematical Formulation

The governing equation of the convection–diffusion equation is expressed as follows:

$$D\Delta u(\mathbf{x}, t) + a(\mathbf{x})\frac{\partial u(\mathbf{x}, t)}{\partial x} + b(\mathbf{x})\frac{\partial u(\mathbf{x}, t)}{\partial y} + c(\mathbf{x})u(\mathbf{x}, t) = \frac{\partial}{\partial t}u(\mathbf{x}, t), \mathbf{x} \in \Omega, t \in [t_0, t_f], \quad (1)$$

where $D$ is the diffusivity coefficient; $\Delta$ represents the Laplace operator; $u(\mathbf{x}, t)$ is to be determined; $a(\mathbf{x})$, $b(\mathbf{x})$, and $c(\mathbf{x})$ are given functions; $t_0$ and $t_f$ denote the initial and final times, respectively; and $\Omega$ is a bounded domain with boundary $\partial\Omega$. The initial condition is adopted using the following equation:

$$u(\mathbf{x}, t = 0) = u_0(\mathbf{x}, 0), \quad (2)$$

where $u_0$ denotes the initial value. The boundary condition is expressed as

$$u(\mathbf{x}, t) = g(\mathbf{x}, t), t_0 \leq t \leq t_f, \quad (3)$$

where $g(\mathbf{x}, t)$ denotes the known function. Equation (1) can be regarded as a steady-state problem if $\partial u(\mathbf{x}, t)/\partial t = 0$. The unknown $\partial u(\mathbf{x}, t)$ can be expressed using the RBF as

$$u(\mathbf{x}, t) = \sum_{j=1}^{M} \lambda_j \varphi_j(\mathbf{x}), \; j = 1, \, 2, \ldots, M, \quad (4)$$

where $\varphi_j$ denotes the RBF and $\lambda_j$ represents unknown vectors for $j = 1, 2, \ldots, M$. $M = M_I + M_B$, where $M$ is the total number of boundary and internal points; $M_I$ is the internal point number; and $M_B$ is the boundary point number. Herein, we propose the following transient radial polynomial series function (TRPSF) as the RBF:

$$\varphi_j(\mathbf{x}, t) = \sum_{k=1}^{M_o} e^{-kt} r_j^{k+2},$$ (5)

where $M_o$ denotes the terms for the TRPSF, and $k$ is the order of the TRPSF. In the proposed method, the approximate solution for $u(x, t)$ can be obtained through the linear combination of the TRPSF, expressed as

$$u(x, t) = \sum_{j=1}^{M_s} \sum_{k=1}^{M_o} \lambda_{j,k} e^{-kt} r_j^{k+2},$$ (6)

where $M_s$ is source point number. The first derivative of $x$ and $y$ for Equation (6) is expressed as

$$\frac{\partial u}{\partial x} = \sum_{j=1}^{M_s} \left( \sum_{k=1}^{M_o} \lambda_{j,k} e^{-kt} (k+2)(x - x_j) r_j^k \right),$$ (7)

$$\frac{\partial u}{\partial y} = \sum_{j=1}^{M_s} \left( \sum_{k=1}^{M_o} \lambda_{j,k} e^{-kt} (k+2)(y - y_j) r_j^k \right).$$ (8)

Similarly, we obtain the second derivative of $x$ and $y$ for Equations (7) and (8) as

$$\frac{\partial^2 u}{\partial x^2} = \sum_{j=1}^{M_s} \left( \sum_{k=1}^{M_o} \lambda_{j,k} e^{-kt} \left( (k+2) r_j^k + k(k+2)(x - x_j)^2 r_j^{k-2} \right) \right),$$ (9)

$$\frac{\partial^2 u}{\partial y^2} = \sum_{j=1}^{M_s} \left( \sum_{k=1}^{M_o} \lambda_{j,k} e^{-kt} \left( (k+2) r_j^k + k(k+2)(y - y_j)^2 r_j^{k-2} \right) \right).$$ (10)

The first derivative of $t$ for Equation (6) is expressed as

$$\frac{\partial u}{\partial t} = \sum_{j=1}^{M_s} \left( \sum_{k=1}^{M_o} \lambda_{j,k} \left( e^{-kt} (k+2)(t - t_j) - k e^{-kt} r_j^{k+2} \right) \right).$$ (11)

The convection–diffusion equation can then be rewritten as follows:

$$\begin{aligned}
&\sum_{j=1}^{M_s} \left( \sum_{k=1}^{M_o} \lambda_{j,k} e^{-kt} (k+2)(k+2) r_j^k \right) + a(\mathbf{x}) \sum_{j=1}^{M_s} \left( \sum_{k=1}^{M_o} \lambda_{j,k} e^{-kt} (k+2)(x - x_j) r_j^k \right) \\
&+ b(\mathbf{x}) \sum_{j=1}^{M_s} \left( \sum_{k=1}^{M_o} \lambda_{j,k} e^{-kt} (k+2)(y - y_j) r_j^k \right) + c(\mathbf{x}) \sum_{j=1}^{M_s} \left( \sum_{k=1}^{M_o} \lambda_{j,k} e^{-kt} r_j^{k+2} \right) \\
&- \sum_{j=1}^{M_s} \left( \sum_{k=1}^{M_o} \lambda_{j,k} \left( e^{-kt} (k+2)(t - t_j) - k e^{-kt} r_j^{k+2} \right) \right) = 0
\end{aligned}$$ (12)

The Dirichlet boundary conditions can be expressed as follows:

$$\sum_{j=1}^{M_s} \sum_{k=1}^{M_o} \lambda_{j,k} e^{-kt} r_j^{k+2} = g(\mathbf{x}_j).$$ (13)

The following system can be obtained by using Equations (12) and (13):

$$\mathbf{P}\boldsymbol{\lambda} = \mathbf{B},\tag{14}$$

in which $\mathbf{P}$ represents a matrix (size of $M \times N$) from the TRPSF, in which $M = M_I + M_B$ and $N = M_o \times M_s$. $\boldsymbol{\lambda}$ denotes an $N \times 1$ vector of unknowns to be determined, and $\mathbf{B}$ represents an $M \times 1$ vector. This study used MATLAB for programing. To solve the system of linear equations, the backslash operator in MATLAB was adopted. The root mean square error (RMSE) was adopted to measure the accuracy of the obtained approximations and defined as follows:

$$\text{RMSE} = \sqrt{\frac{1}{n_t} \sum_{i=1}^{n_t} (\hat{u}(x_i) - u(x_i))^2},\tag{15}$$

where $n_t$ represents the number of internal points and $u(x_i)$ and $\hat{u}(x_i)$ are the exact and approximate solutions at the $i^{th}$ collocation point, respectively.

## 3. Validation and Convergence Analysis

To validate the proposed approach, we conduct an example and compared the numerical results with other RBFs, namely the Gaussian, MQ, inverse MQ (IMQ) and conical RBFs. The following convection–diffusion equation was considered:

$$D\Delta u + a(\mathbf{x})\frac{\partial u}{\partial x} + b(\mathbf{x})\frac{\partial u}{\partial y} + c(\mathbf{x})u = f(x,y), (x,y) \in \Omega,\tag{16}$$

where $D$ represents the diffusivity coefficient ranging from 0.001 to 1000; $a(\mathbf{x}) = y\cos(x), b(\mathbf{x}) = \sinh(x)$, and $c(\mathbf{x}) = x^2 + y^2$. In Equation (17), $f(x,y)$ can be obtained by substituting the exact solution into Equation (16).

$$\begin{aligned} f(x,y) = &\ D((-\pi^2 + 1)(\sin(\pi x)\cosh(y)) + (\pi^2 - 1)(\cos(\pi x)\sinh(y))) + \\ &\ (y\cos x)(\pi\cos(\pi x)\cosh(y) + \pi\sin(\pi x)\sinh(y)) + \\ &\ \sinh(x)(\sin(\pi x)\sinh(y) - \cos(\pi x)\cosh(y)) + \\ &\ (x^2 + y^2)(\sin(\pi x)\cosh(y) - \cos(\pi x)\sinh(y)). \end{aligned}\tag{17}$$

The boundary $\partial\Omega$ of the irregular domain is defined by the following parametric equation:

$$\partial\Omega = \left\{ (x,y) \big| x = \rho(\theta)\cos\theta, y = \rho(\theta)\sin\theta \right\}, \rho = \left| sec(3\theta)^{\sin 6\theta} \right|, 0 \leq \theta \leq 2\pi.\tag{18}$$

The analytical solution in this example is expressed as

$$u(x,y) = \sin(\pi x)\cosh(y) - \cos(\pi x)\sinh(y).\tag{19}$$

The Dirichlet boundary condition is considered using the analytical solution

$$u(x,y) = \sin(\pi x)\cosh(y) - \cos(\pi x)\sinh(y), (x,y) \in \partial\Omega.\tag{20}$$

In the numerical implementation, the Dirichlet boundary conditions are provided on the boundary by using the analytical solution. We first examined the accuracy of the position of the sources to the results. Two layouts of possible locations for the source points, depicted in Figures 1 and 2, are called the internal and external source collocation schemes, respectively. For the external source space–time collocation scheme, the sources are collocated away from the domain on the basis of the following equation:

$$\mathbf{y}_j = \eta r_j(\cos\theta_j, \sin\theta_j), j = 1,\ldots,M_s,\tag{21}$$

where $\eta$ represents the dilation parameter; $\eta > 1$, $\theta_j$ represents the angle of the source point, and $r_j$ is the radius of the source point.
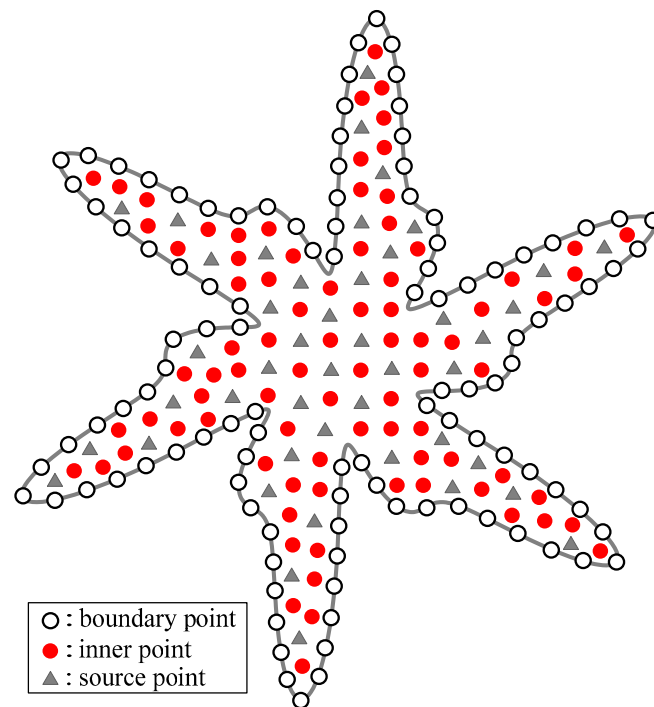


**Figure 1.** Internal source collocation scheme for the proposed method.
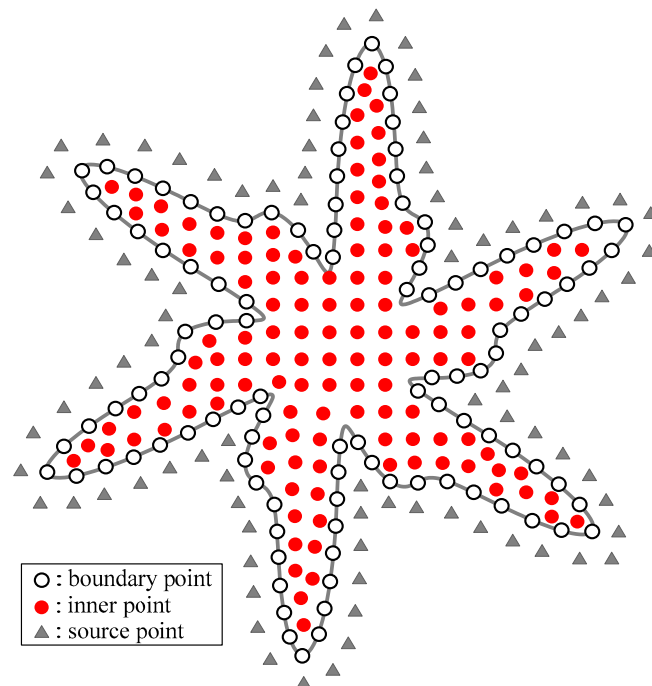


**Figure 2.** External source collocation scheme for the proposed method.

The computed RMSE with respect to the TRPSF terms is plotted in Figure 3. According to Figure 3, the highest accuracy occurred when $M_o > 10$. Moreover, the external source space–time collocation scheme was obviously more accurate than the internal source space–time collocation scheme. Consequently, the proposed method with an external source collocation scheme was adopted in this study. Figure 4 plots the dilation parameter against the RMSE. Highly accurate solutions could

be obtained when the dilation parameter was greater than 4. The convergence analysis demonstrated that the dilation parameter is not sensitive to the accuracy level. Because the presented approach and the radial basis function collocation method (RBFCM) have a similar mathematical background, these methods were adopted to solve the same problem. The RBFCM with the optimal shape parameter was considered using the Gaussian, MQ, IMQ, and conical RBFs. Table 1 presents the results of the example comparison. All cases in Table 1 demonstrate that the proposed method is more accurate than is the conventional RBFCM with the optimal shape parameter. A parameter study when the diffusivity coefficient *D* varies from 0.001 to 1000 was also conducted. Table 2 presents the numerical results with different values by using the RPSF as well as the MQ RBF. More stable and accurate results could be obtained using the numerical model compared with the MQ RBF even when a large range of *D* values is considered. A comparison with the exact solution is presented in Figure 5. The numerical solution is consistent with the analytical solution.
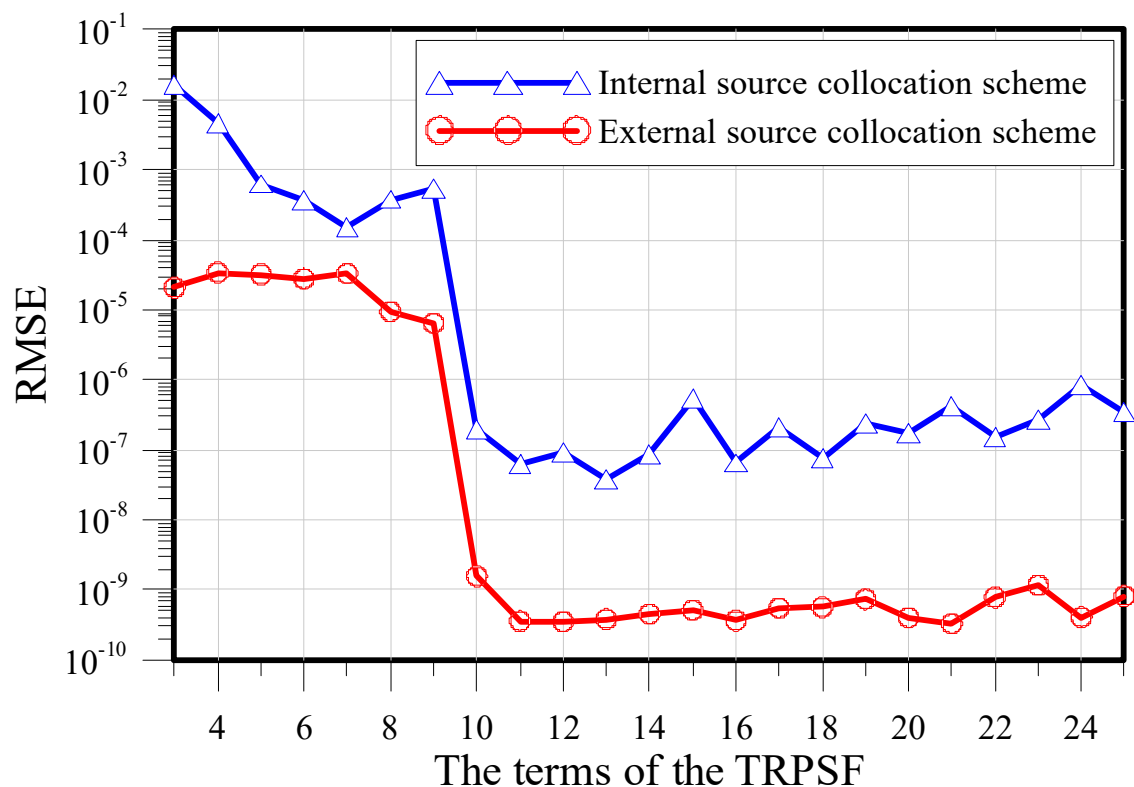


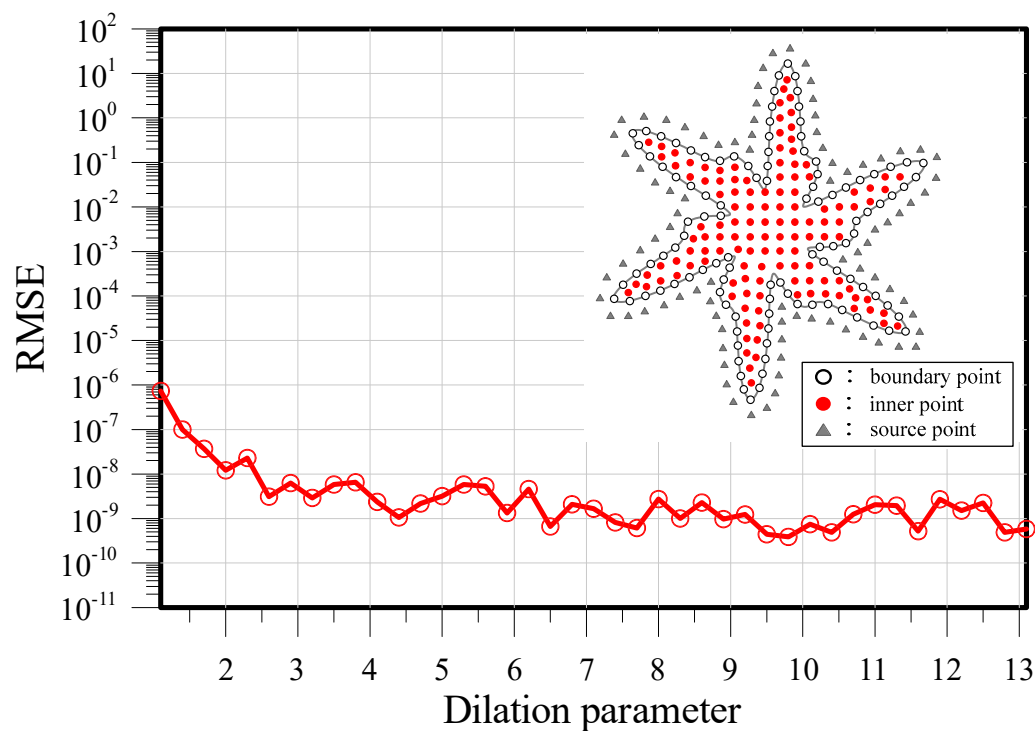**Figure 3.** Transient radial polynomial series function (TRPSF) terms versus RMSE.

**Figure 4.** Dilation parameter versus RMSE.

**Table 1.** Root mean square errors (RMSEs) of the proposed approach and other radial basis functions (RBFs).

| | | RMSE | | | | |
|---|---|---|---|---|---|---|
| $M_B$ | $M_I$ | This Study | Multiquadratic (MQ) RBF | Inverse Multiquadriatic (IMQ) RBF | Gaussian | Conical RBF ($r^9$) |
| 1916 | 514 | $9.53 \times 10^{-10}$ | $2.68 \times 10^{-4}$ ($c = 0.2$) | $1.35 \times 10^{-4}$ ($c = 0.5$) | $5.76 \times 10^{-4}$ ($c = 0.5$) | $2.85 \times 10^{-4}$ |
| 2058 | 642 | $5.85 \times 10^{-10}$ | $2.38 \times 10^{-4}$ ($c = 0.2$) | $1.28 \times 10^{-4}$ ($c = 0.5$) | $5.68 \times 10^{-4}$ ($c = 0.5$) | $2.72 \times 10^{-4}$ |
| 2308 | 982 | $3.88 \times 10^{-10}$ | $2.65 \times 10^{-4}$ ($c = 0.1$) | $1.20 \times 10^{-4}$ ($c = 0.5$) | $5.33 \times 10^{-4}$ ($c = 0.5$) | $2.46 \times 10^{-4}$ |
| 2500 | 1280 | $6.14 \times 10^{-10}$ | $2.47 \times 10^{-4}$ ($c = 0.1$) | $1.41 \times 10^{-4}$ ($c = 0.5$) | $5.07 \times 10^{-4}$ ($c = 0.5$) | $1.86 \times 10^{-4}$ |
| 2642 | 1678 | $2.63 \times 10^{-10}$ | $2.12 \times 10^{-4}$ ($c = 0.1$) | $1.30 \times 10^{-4}$ ($c = 0.6$) | $4.86 \times 10^{-4}$ ($c = 0.5$) | $1.76 \times 10^{-4}$ |
| 2761 | 2369 | $7.65 \times 10^{-10}$ | $2.40 \times 10^{-4}$ ($c = 0.1$) | $1.29 \times 10^{-4}$ ($c = 0.5$) | $4.57 \times 10^{-4}$ ($c = 0.5$) | $1.35 \times 10^{-4}$ |

**Table 2.** RMSE of the proposed approach and the MQ RBF for the diffusivity of the coefficient.

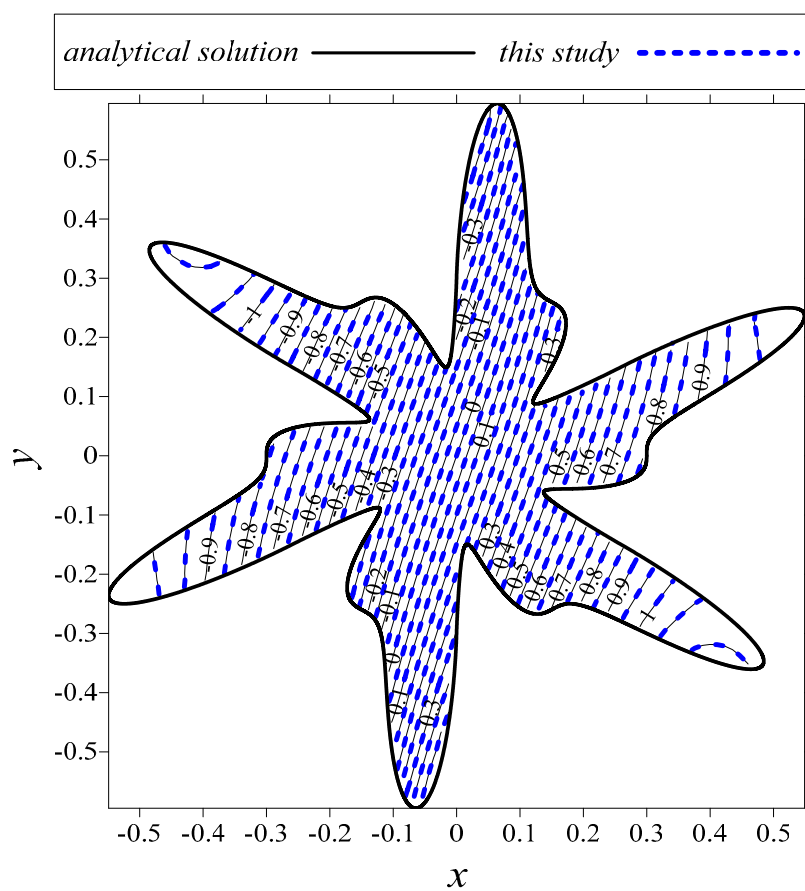| | RMSE | |
|---|---|---|
| $D$ | This Study | MQ RBF |
| 0.001 | $4.74 \times 10^{-10}$ | $2.22 \times 10^{-5}$ ($c = 0.55$) |
| 0.01 | $4.22 \times 10^{-10}$ | $2.69 \times 10^{-5}$ ($c = 0.60$) |
| 0.1 | $3.46 \times 10^{-10}$ | $6.01 \times 10^{-6}$ ($c = 0.55$) |
| 1 | $5.71 \times 10^{-10}$ | $1.41 \times 10^{-5}$ ($c = 0.65$) |
| 10 | $6.11 \times 10^{-10}$ | $4.07 \times 10^{-4}$ ($c = 0.55$) |
| 100 | $3.02 \times 10^{-9}$ | $2.78 \times 10^{-4}$ ($c = 2.90$) |
| 1000 | $1.26 \times 10^{-8}$ | $7.80 \times 10^{-4}$ ($c = 4.55$) |

**Figure 5.** Comparison of the numerical solution with the analytical solution.

The second example was a stationary problem enclosed by a Cassini–shaped domain, as depicted in Figure 6. The governing equation is as follows:

$$D\Delta u + a(\mathbf{x})\frac{\partial u}{\partial x} + b(\mathbf{x})\frac{\partial u}{\partial y} + c(\mathbf{x})u = f(x,y), (x,y) \in \Omega, \tag{22}$$

where $D = 1$; $a(\mathbf{x}) = xy + x^2$; $b(\mathbf{x}) = x\sinh(y)$; and $c(\mathbf{x}) = \sin(x+y)$. $f(x,y)$ can be obtained by substituting the exact solution into Equation (22) as follows:

$$f(x,y) = 2e^{x+y} + (xy + x^2)e^{x+y} + x\sinh(y)e^{x+y} + \sin(x+y)e^{x+y}. \tag{23}$$

The Cassini–shaped domain is expressed as

$$\partial\Omega = \left\{(x,y)\big|x = \rho(\theta)\cos\theta, y = \rho(\theta)\sin\theta\right\}, \rho(\theta) = \left(\cos(3\theta) + \sqrt{2 - \sin^2(3\theta)}\right)^{1/3}, 0 \leq \theta \leq 2\pi. \tag{24}$$

The Dirichlet boundary condition is applied using the following analytical solution:
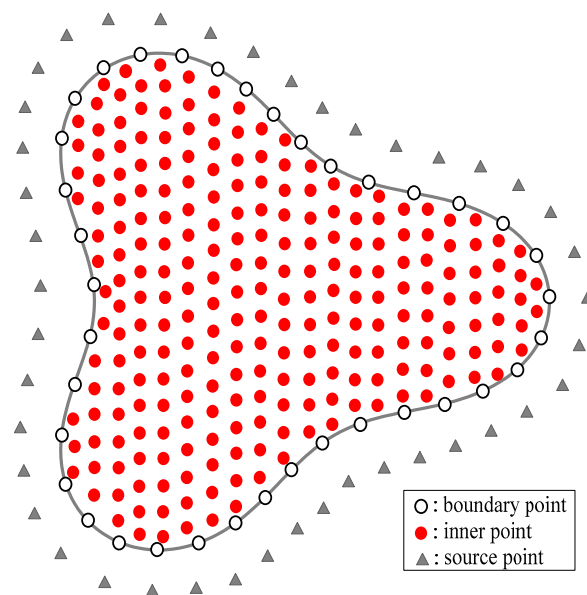
$$u(x,y) = e^{x+y}. \tag{25}$$

**Figure 6.** Layout of collocation points.

The Dirichlet boundary condition is imposed on the Cassini–shaped domain by using the analytical solution. The layout of the collocation points is presented in Figure 6. Figure 7 depicts the computed results with the analytical solution. The convergence analysis of the presented approach was conducted with different TRPSF terms. Figure 8 demonstrates that the RMSE is decreases as the RPSF terms increase. Highly accurate results could be obtained when the TRPSF terms were greater than 9. Figure 9 presents the dilation parameter versus the RMSE. Similar to that of the previous example, the convergence analysis of the present example demonstrated that the dilation parameter is not sensitive to accuracy. A convergence analysis of the collocation point number was performed. The RMSE decreased as the number of boundary and internal points increased, as presented in Figures 10 and 11. In summary, highly accurate results could be obtained using the proposed method.
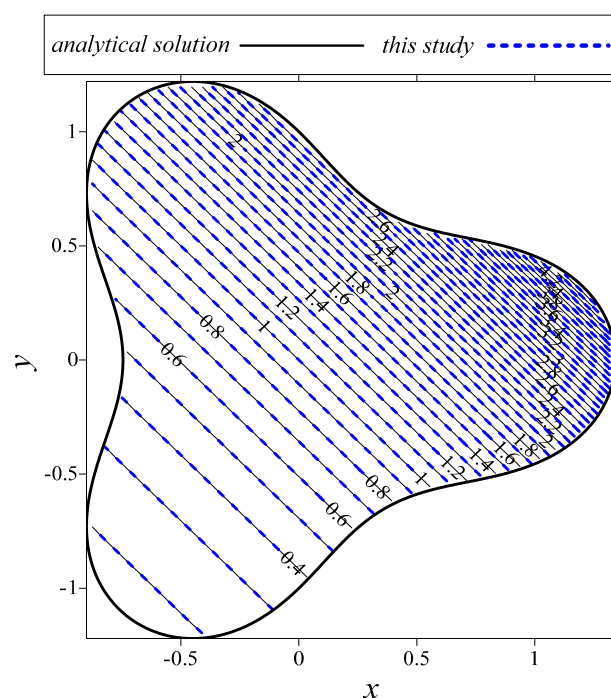


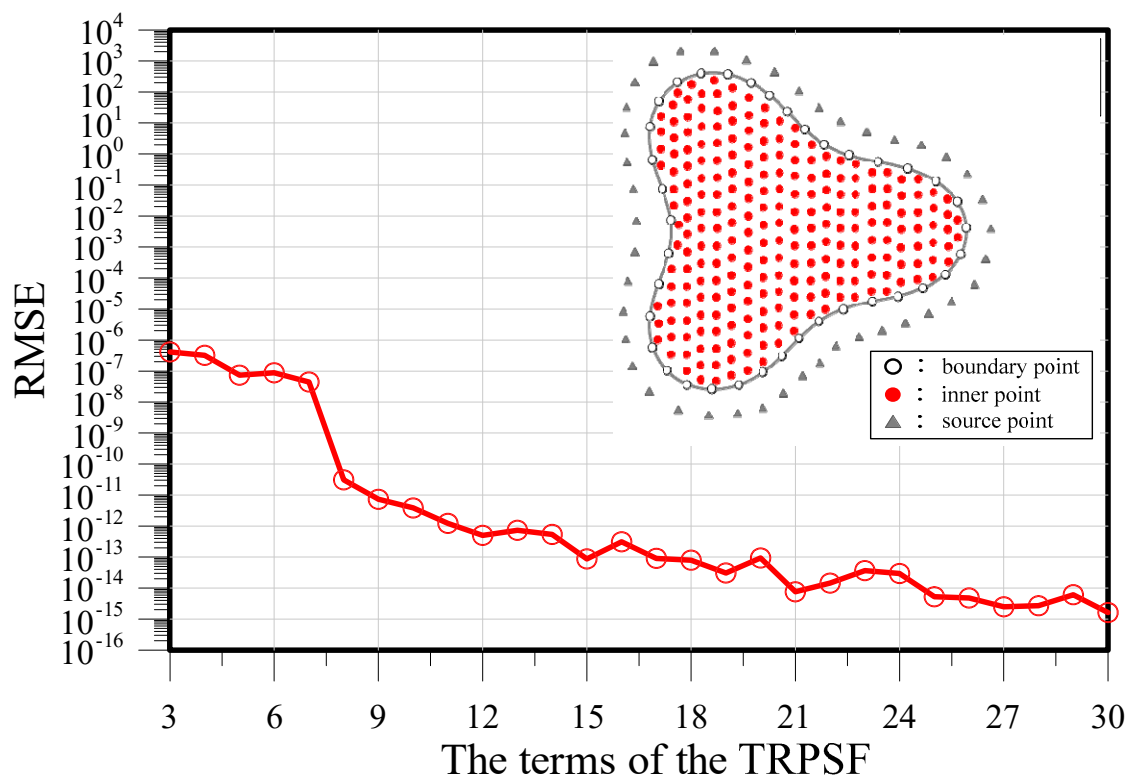**Figure 7.** Comparison of the numerical solution with the exact solution.
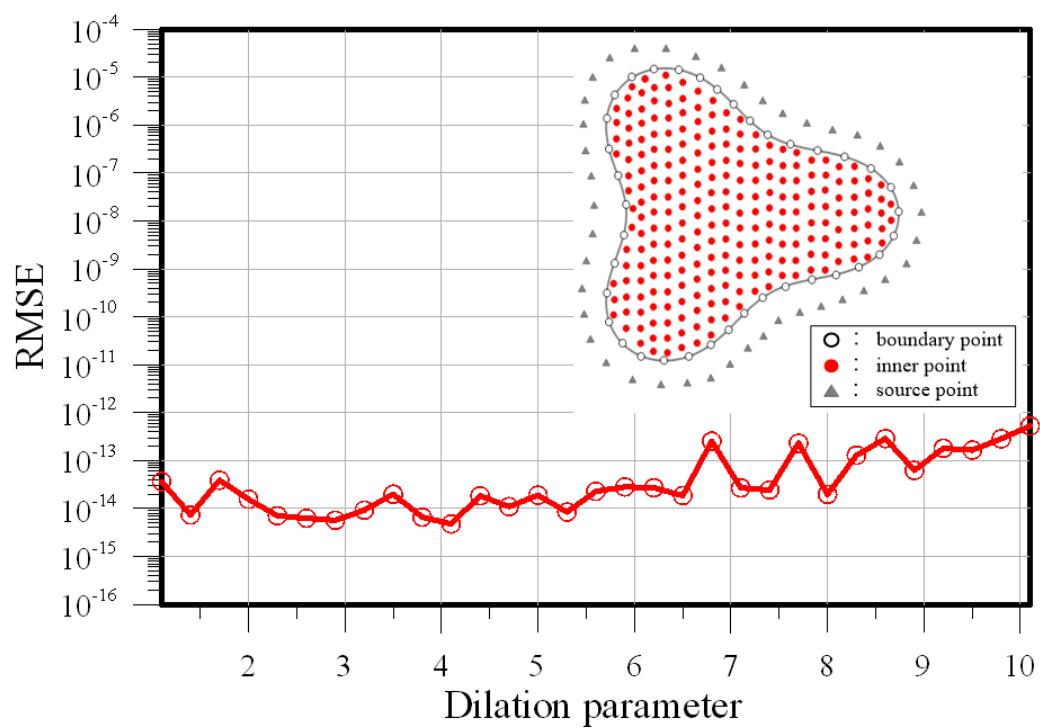
**Figure 8.** TRPSF terms versus RMSE.



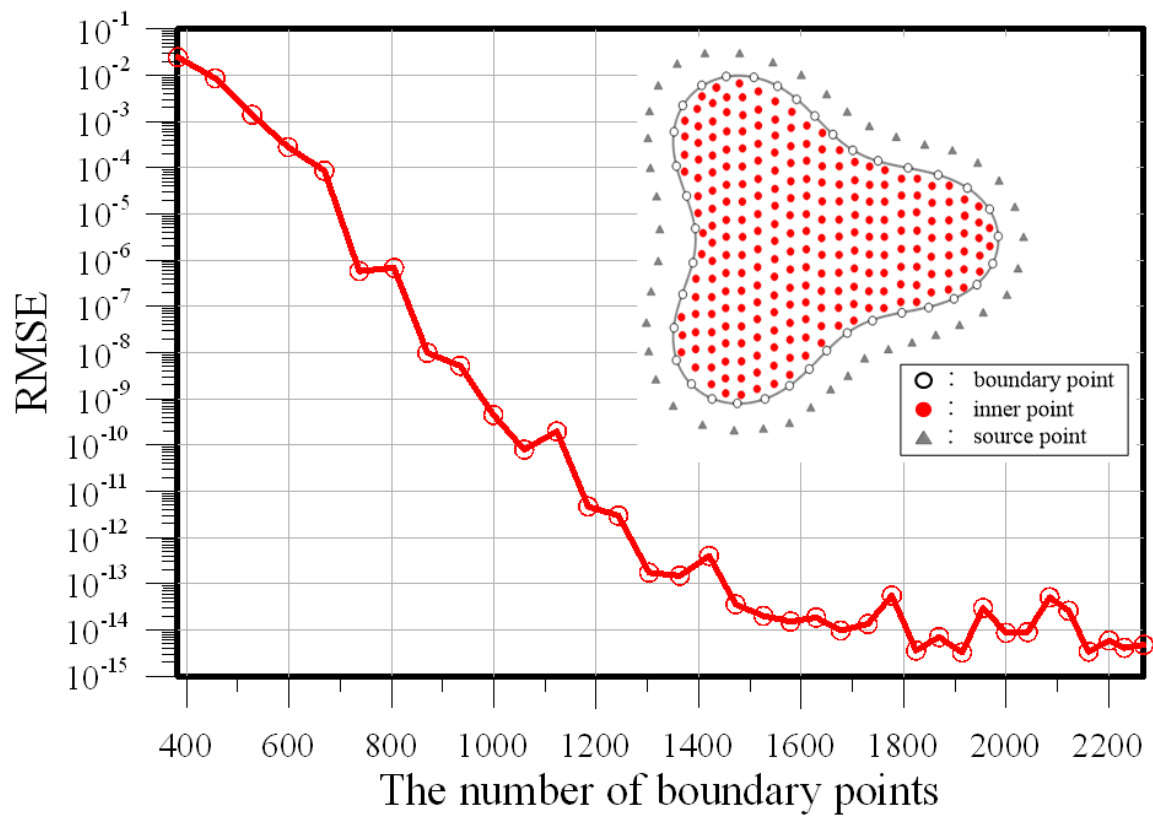**Figure 9.** Dilation parameter versus RMSE.

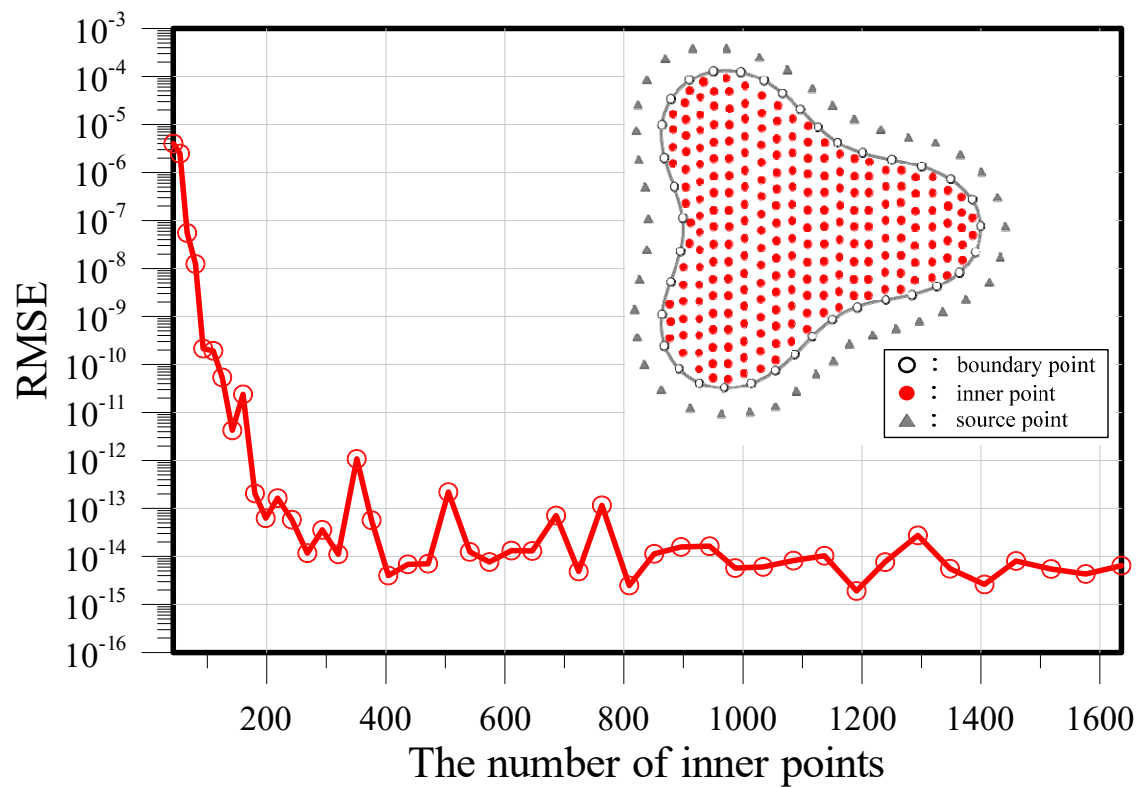**Figure 10.** Number of boundary points versus RMSE.



**Figure 11.** Number of inner points versus RMSE.

## 4. Numerical Examples.

*4.1. Diffusion Equation Modeling in Two Dimensions*

In this example, the numerical solution of the time-dependent diffusion equation was investigated. Because the proposed method is advantageous for domains with complicated shapes, a problem with a gear-like shape was used. Consider the following governing equation:

$$D\Delta u(\mathbf{x},t) = \frac{\partial}{\partial t}u(\mathbf{x},t), \mathbf{x} \in \Omega, t \in [t_0, t_f], \tag{26}$$

where $D = 1$. The two–dimensional object boundary is expressed as

$$\partial\Omega = \left\{ (x,y) \middle| x = \rho(\theta)\cos\theta, y = \rho(\theta)\sin\theta \right\}, \rho(\theta) = 1 + \frac{1}{10}\tanh(10\sin(12\theta)), 0 \le \theta \le 2\pi. \tag{27}$$

Given the initial data,

$$u(\mathbf{x}, t = 0) = \sin(x)\cos(y). \tag{28}$$

The Dirichlet boundary condition is imposed on the boundary by using Equation (29).

$$u(\mathbf{x},t) = e^{-2t}\sin(x)\cos(y). \tag{29}$$

In this case, there are 8 TRPSF terms. The final elapsed time under consideration is from 1 to 5. The numbers of source, boundary, and internal points were 312, 478, and 1392, respectively. The diffusivity coefficient is 1. Figure 12a shows the original two-dimensional problem enclosed by a gear-like shape. Without consideration of the time-marching algorithm, we transformed the domain of the two-dimensional problem into a three-dimensional space–time domain, as depicted in Figure 12b. Table 3 lists the RMSE for dilation parameters ranging from 1.5–6.5 as well as at different elapsed times. Highly accurate results could be obtained in the presented approach.

**Table 3.** RMSEs for different $\eta$ values.

| Time | $\eta$=1.5 | $\eta$=3.0 | $\eta$=4.5 | $\eta$=5.0 | $\eta$=6.5 |
|------|-----------|-----------|-----------|-----------|-----------|
| $t = 1.0$ | $1.24 \times 10^{-9}$ | $7.90 \times 10^{-9}$ | $5.56 \times 10^{-8}$ | $1.01 \times 10^{-7}$ | $2.97 \times 10^{-7}$ |
| $t = 2.0$ | $2.78 \times 10^{-8}$ | $8.80 \times 10^{-8}$ | $8.57 \times 10^{-8}$ | $3.26 \times 10^{-7}$ | $5.18 \times 10^{-7}$ |
| $t = 3.0$ | $3.42 \times 10^{-8}$ | $8.91 \times 10^{-8}$ | $1.67 \times 10^{-7}$ | $6.16 \times 10^{-7}$ | $4.12 \times 10^{-7}$ |
| $t = 4.0$ | $1.77 \times 10^{-7}$ | $2.75 \times 10^{-7}$ | $5.38 \times 10^{-7}$ | $1.67 \times 10^{-7}$ | $3.58 \times 10^{-7}$ |
| $t = 5.0$ | $6.69 \times 10^{-7}$ | $2.92 \times 10^{-7}$ | $2.21 \times 10^{-7}$ | $2.23 \times 10^{-7}$ | $2.98 \times 10^{-7}$ |

(**a**)



(**b**)

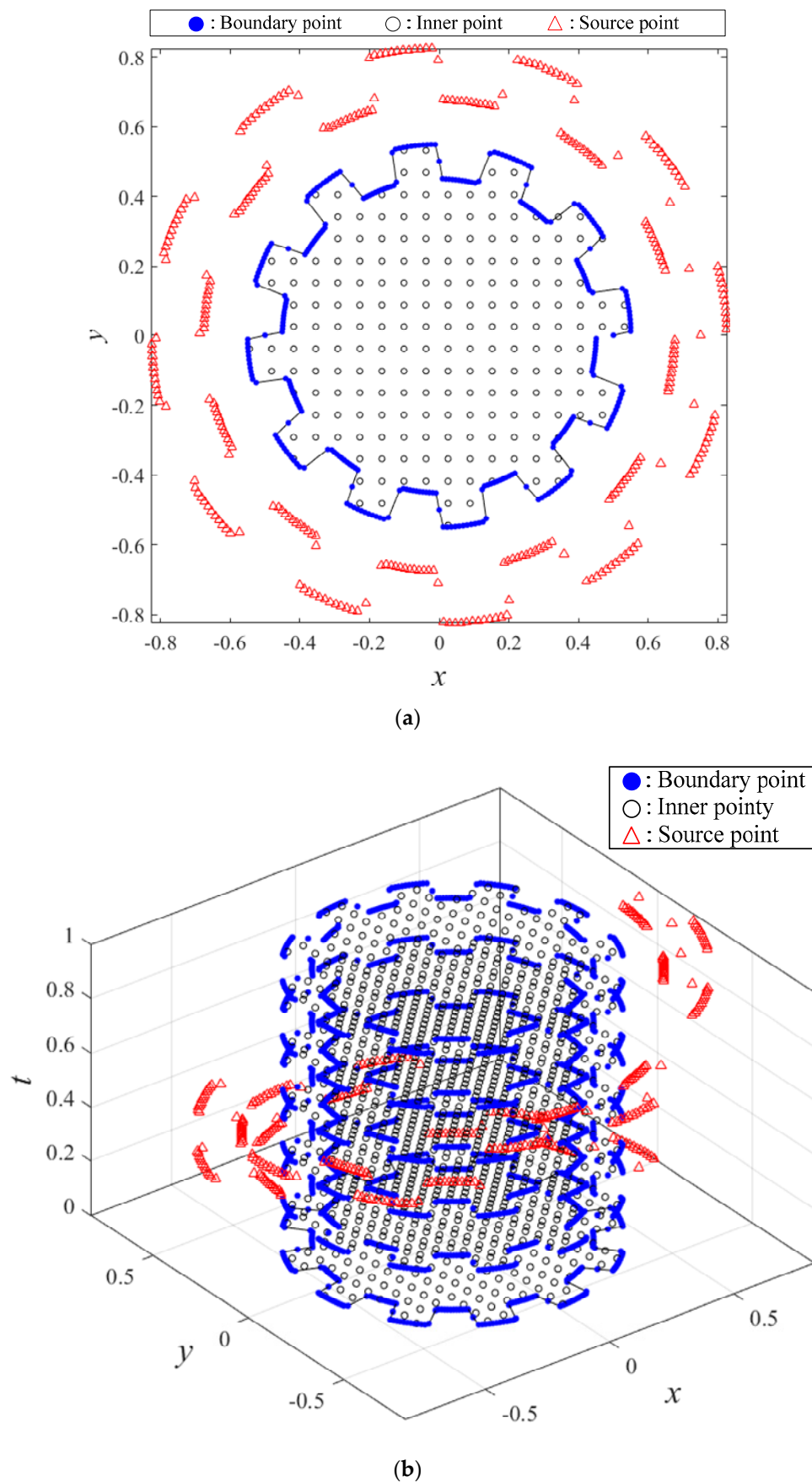**Figure 12.** Collocation scheme of the proposed approach for example 4.1 projected on (**a**) an *x*–*y* plane and (**b**) space–time coordinates.

### 4.2. Modeling the Two-Dimensional Convection–Diffusion Equation: Case 1

In this example, the numerical solution of the convection–diffusion equation was investigated. The governing equation is expressed as

$$D\Delta u(\mathbf{x},t) + a(\mathbf{x})\frac{\partial u(\mathbf{x},t)}{\partial x} + b(\mathbf{x})\frac{\partial u(\mathbf{x},t)}{\partial y} + f(\mathbf{x},t) = \frac{\partial}{\partial t}u(\mathbf{x},t), \mathbf{x}\in\Omega, t\in[t_0,t_f], \tag{30}$$

where $D = 1$, $a(\mathbf{x}) = -\cos(y)$, and $b(\mathbf{x}) = -\sin(x)$; $f(\mathbf{x},t)$ can be obtained on the basis of the exact solution as

$$f(\mathbf{x},t) = \sin(x)\sin(y)(-\sin(t) + 2D\cos(t)) + \cos(t)(\cos(y)\cos(x)\sin(y) + \sin(x)\sin(x)\cos(y)). \tag{31}$$

The two-dimensional parametric equation is expressed as follows:

$$\partial\Omega = \left\{(x,y,t)\big|x = \rho(\theta)\cos\theta, y = \rho(\theta)\sin\theta\right\}, \rho(\theta) = \frac{3 + \cos(\theta - \pi/7)\sin(4\theta)}{5 + \sin(2\theta)}, 0\leq\theta\leq 2\pi. \tag{32}$$

Given the initial boundary conditions,

$$u(\mathbf{x}, t = 0) = \sin(x)\sin(y). \tag{33}$$

The Dirichlet data is designated on the boundary by adopting Equation (34).

$$u(\mathbf{x},t) = \sin(x)\sin(y)\cos(t). \tag{34}$$

In this case, there are eight TRPSF terms. The final elapsed time is 1, and the diffusivity coefficient is 1. Figure 13a presents the original two-dimensional problem enclosed in an irregular shape. Figure 13b presents the proposed three-dimensional space–time domain. We collocated the source points outside the domain, and the dilation parameter was set to 2.8. To verify the accuracy of the proposed method, several cases with various collocation points were used, as presented in Table 4. Table 4 also shows the comparison of this study, the RBFCM using MQ RBF with the implicit scheme and the space–time meshless method (STMM) [32]. The central processing unit (CPU) times recorded from a computer using an 3.60–GHz Intel Core i7–7700 CPU (ASUSTeK Computer Inc., Taipei, Taiwan) are also listed in Table 4. The step size for the MQ RBF with the time-marching scheme was set to 0.1. More accurate results could be obtained using the proposed method compared with other methods.
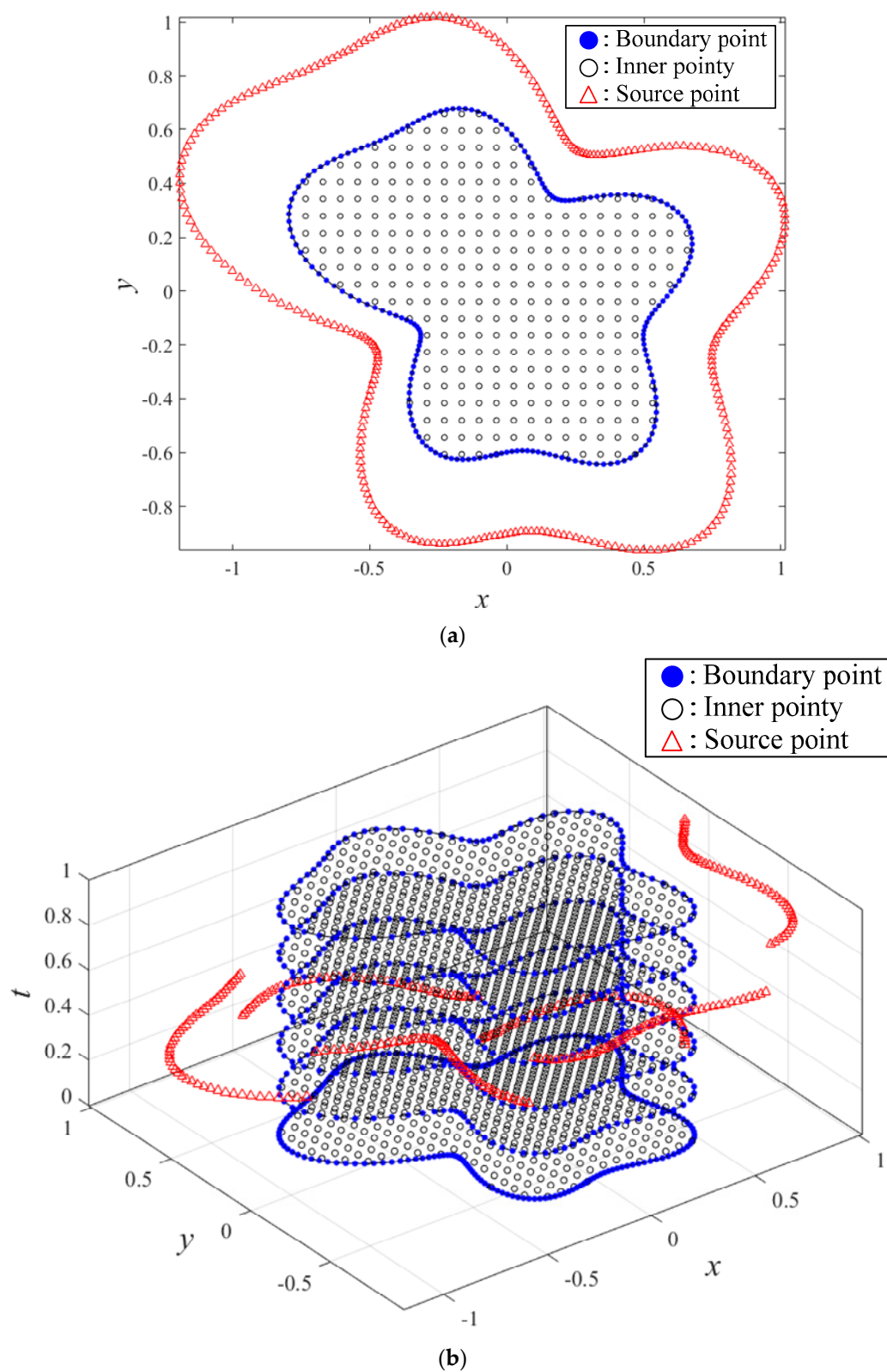
**Figure 13.** Collocation scheme of the proposed approach for example 4.2 projected on (**a**) an *x–y* plane and (**b**) space–time coordinates.

**Table 4.** RMSEs and CPU times of the presented method and the MQ radial basis function (RBF).

| $M$ | This Study | | MQ RBF | | STRBF [32] |
|---|---|---|---|---|---|
| | $t = 0.5$ | $t = 1.0$ | $t = 0.5$ | $t = 1.0$ | $t = 0.5$ |
| 517 | $2.79 \times 10^{-5}$ (0.72 s) | $5.65 \times 10^{-5}$ (0.75 s) | $5.55 \times 10^{-4}$ (0.74 s) | $2.04 \times 10^{-3}$ (1.05 s) | $5.64 \times 10^{-3}$ |
| 987 | $2.69 \times 10^{-7}$ (2.77 s) | $3.99 \times 10^{-7}$ (2.88 s) | $4.00 \times 10^{-4}$ (3.05 s) | $1.47 \times 10^{-3}$ (4.43 s) | $8.48 \times 10^{-4}$ |
| 1722 | $5.45 \times 10^{-8}$ (15.55 s) | $1.15 \times 10^{-6}$ (16.05 s) | $2.99 \times 10^{-4}$ (16.22 s) | $1.10 \times 10^{-3}$ (25.43 s) | $1.94 \times 10^{-4}$ |
| 2730 | $1.82 \times 10^{-8}$ (64.08 s) | $1.53 \times 10^{-7}$ (65.11 s) | $2.36 \times 10^{-4}$ (74.82 s) | $8.68 \times 10^{-4}$ (100.81 s) | $6.04 \times 10^{-5}$ |
| 3380 | $3.93 \times 10^{-8}$ (133.71 s) | $5.56 \times 10^{-7}$ (135.43 s) | $2.10 \times 10^{-4}$ (146.92 s) | $7.75 \times 10^{-4}$ (217.36 s) | $4.92 \times 10^{-5}$ |
| 4179 | $3.02 \times 10^{-8}$ (249.42 s) | $3.29 \times 10^{-7}$ (253.92 s) | $1.89 \times 10^{-4}$ (258.64 s) | $6.98 \times 10^{-4}$ (378.69 s) | $3.41 \times 10^{-5}$ |

Note: $M = M_I + M_B$ denotes the sum of the boundary and inner point numbers. The step size for the MQ RBF with the time–marching scheme was set to 0.1.

### 4.3. Modeling the Two-Dimensional Convection–Diffusion Equation: Case 2

The final investigated example was the numerical solution of the convection–diffusion equation. The governing equation is expressed as follows:

$$D\Delta u(\mathbf{x}, t) + a(\mathbf{x})\frac{\partial u(\mathbf{x}, t)}{\partial x} + b(\mathbf{x})\frac{\partial u(\mathbf{x}, t)}{\partial y} + f(\mathbf{x}, t) = \frac{\partial}{\partial t}u(\mathbf{x}, t), \mathbf{x} \in \Omega, t \in [t_0, t_f], \tag{35}$$

where $D = 1$, $a(\mathbf{x}) = x\sin(y)$, and $b(\mathbf{x}) = y\cos(x)$; $f(\mathbf{x}, t)$ can be obtained on the basis of the exact solution as

$$f(\mathbf{x}, t) = (y\sin(x) + x\cos(y))(D\cos(t) - \sin(t)) - (x\sin(y)\cos(t))(y\cos(x) + \cos(y)) \\ -(y\cos(x)\cos(t))(\sin(x) - x\sin(y)) \tag{36}$$

The two-dimensional parametric equation is expressed as follows:

$$\partial\Omega = \{(x, y, t)|x = \rho(\theta)\cos\theta, y = \rho(\theta)\sin\theta\}, \rho(\theta) = 1 + (\cos(4\theta))^2, 0 \leq \theta \leq 2\pi. \tag{37}$$

The initial conditions are expressed as

$$u(\mathbf{x}, t = 0) = y\sin(x) + x\cos(y). \tag{38}$$

We imposed the Dirichlet boundary condition on the boundary by using Equation (39).

$$u(\mathbf{x}, t) = (y\sin(x) + x\cos(y))\cos(t). \tag{39}$$

In this case, the TRPSF has eight terms and the final elapsed time is 1. The numbers of source, boundary, and internal points are 264, 778 and 1032, respectively. The diffusivity coefficient is 1. Figure 14a presents the original two-dimensional problem enclosed by a star-like shape. Figure 14b presents the proposed three-dimensional space–time domain. In this case, the dilation parameter is set to 1.2. A convergence analysis of the number of boundary and internal points was performed. The RMSE decreased as the number of boundary and internal points increased, as depicted in Figures 15 and 16. Additionally, highly accurate results were obtained using the proposed method for the numerical solution of the two-dimensional time-dependent convection–diffusion equation. Figure 17 compares the computed solutions with the exact solution at different times and indicates suitable agreement.
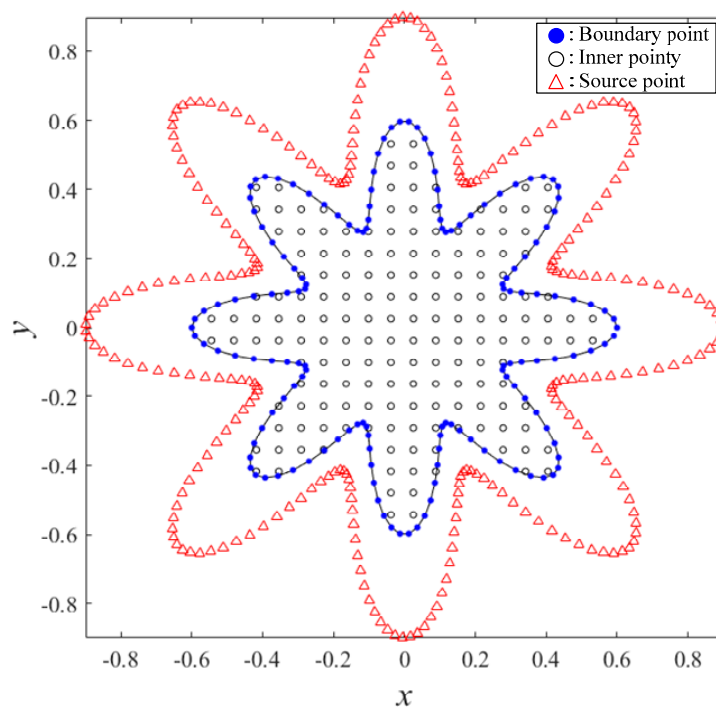
(**a**)
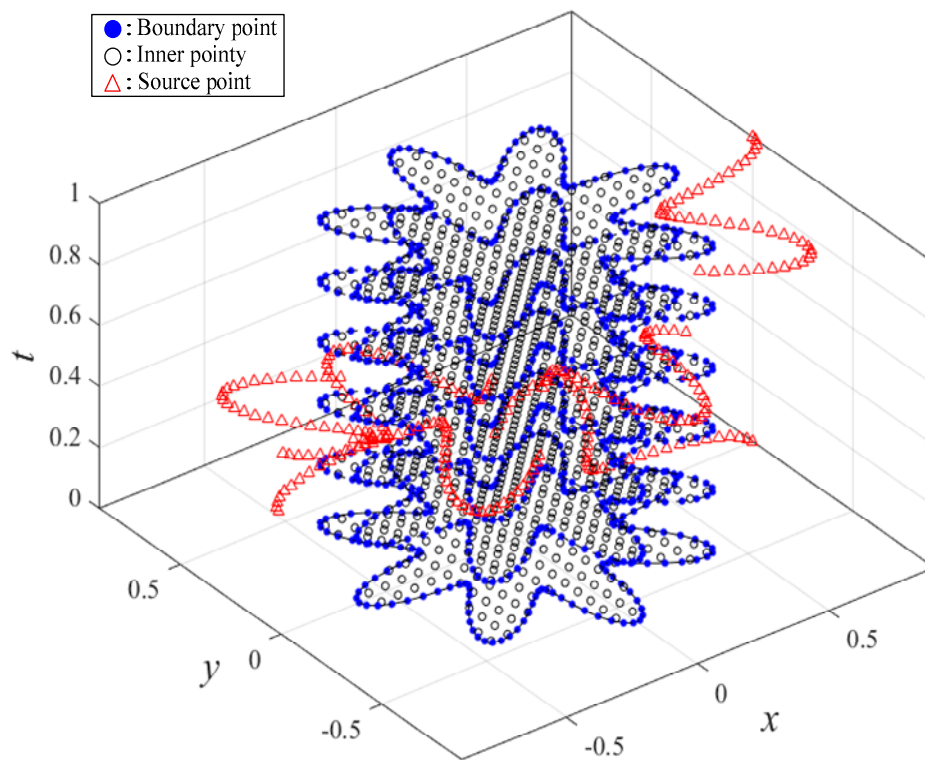


(**b**)

**Figure 14.** Collocation scheme of the proposed approach for example 4.3 projected on (**a**) an *x*–*y* plane and (**b**) space–time coordinates.
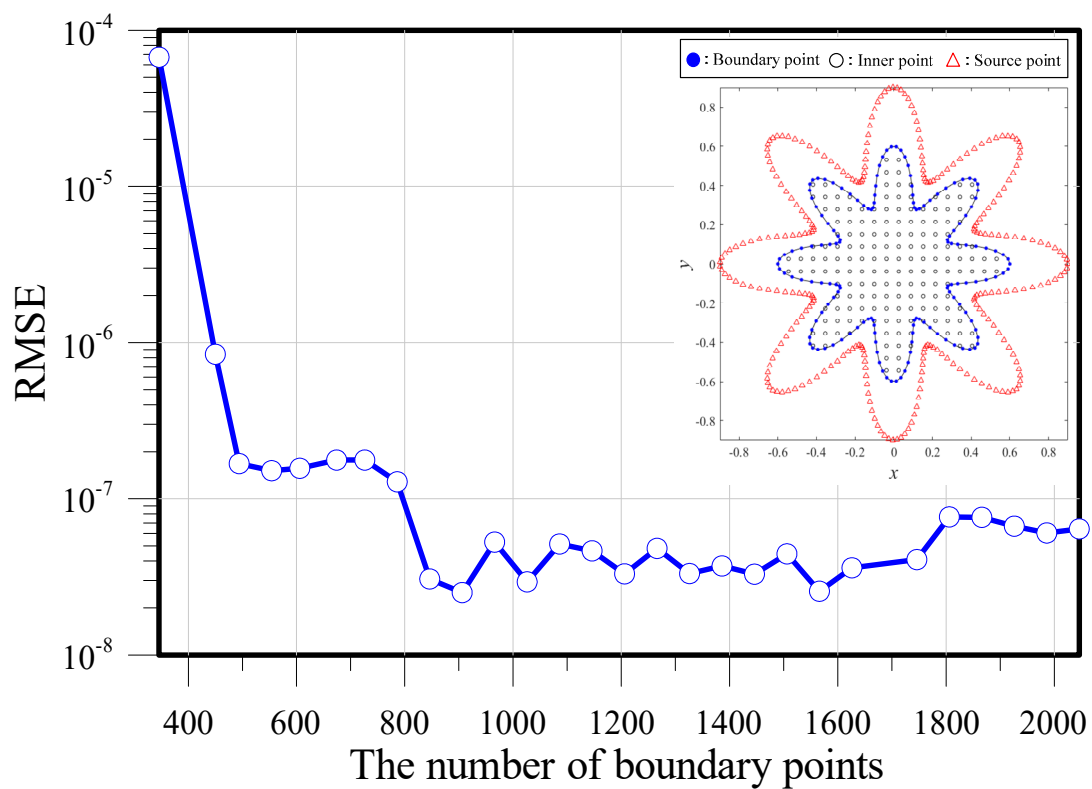
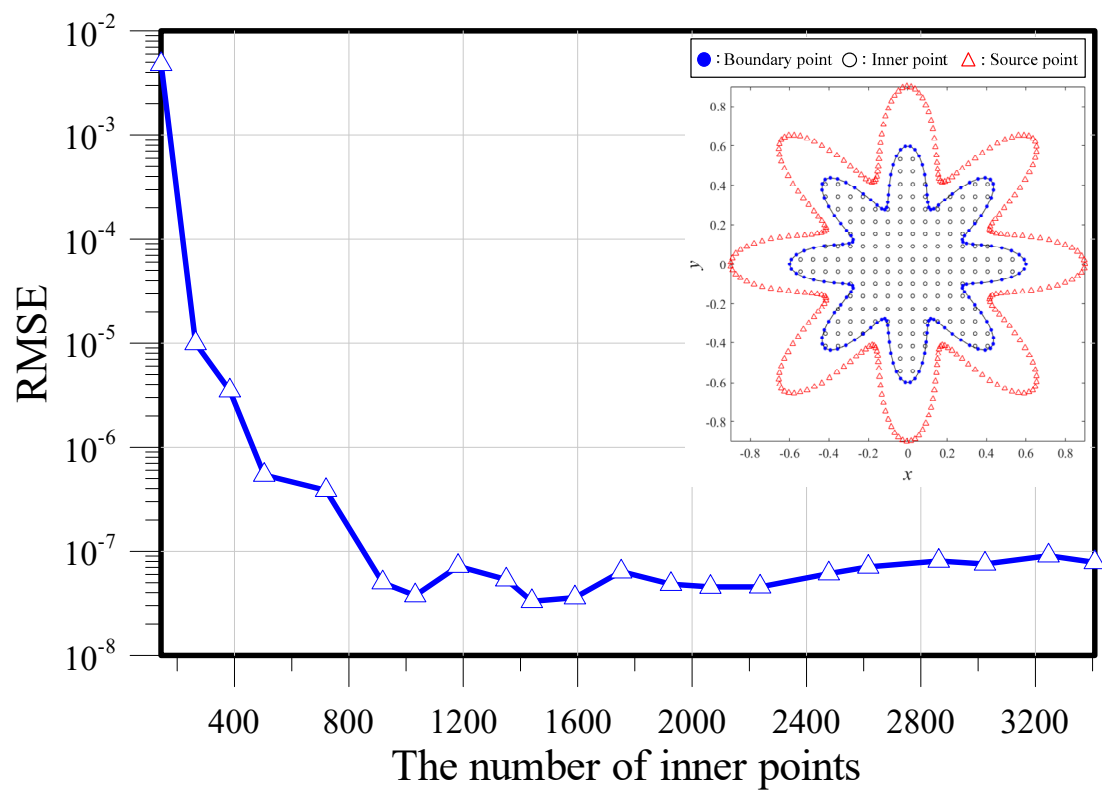**Figure 15.** Boundary point number versus RMSE.
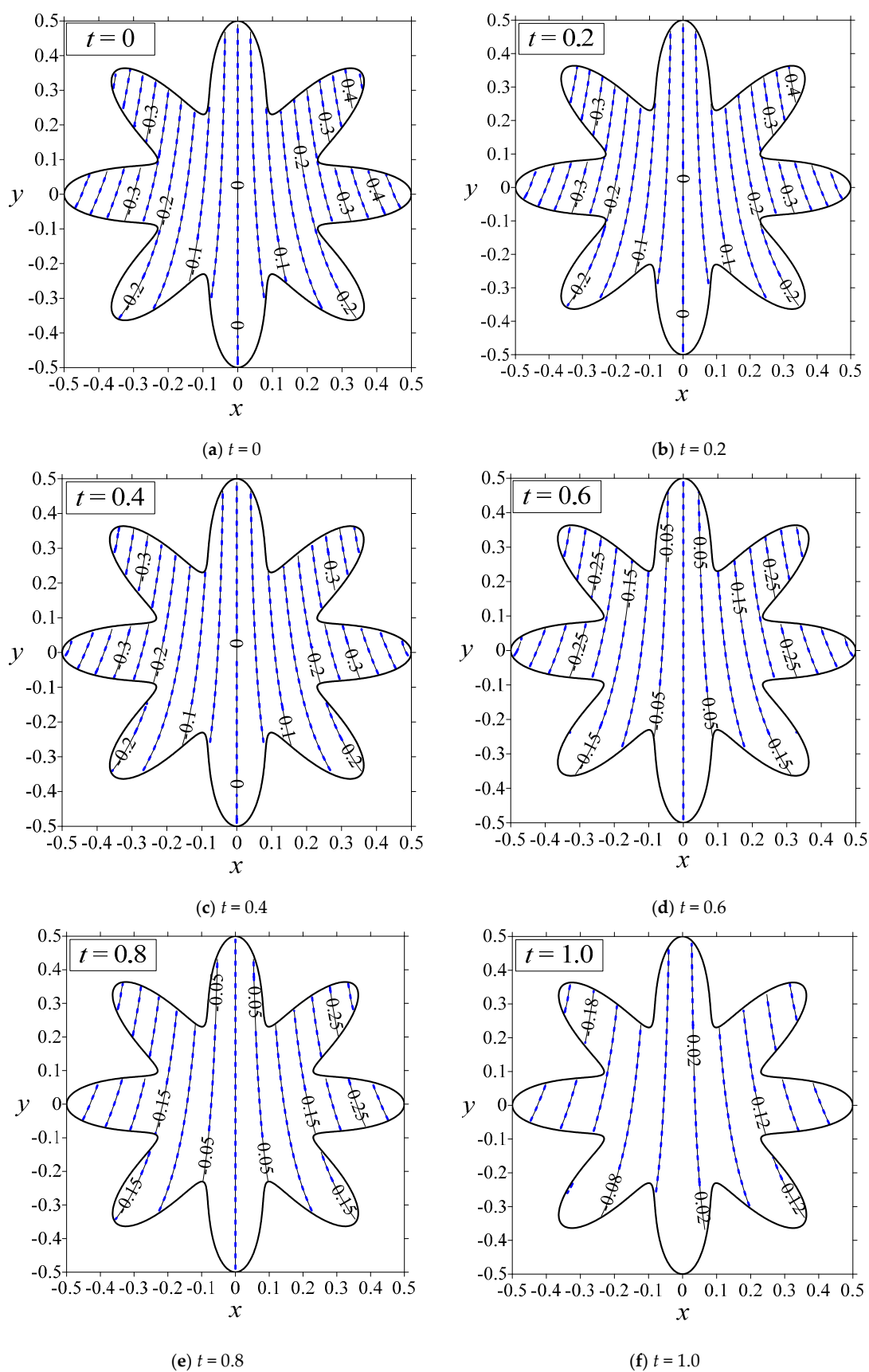


**Figure 16.** Internal point number versus RMSE.

(**a**) *t* = 0

(**b**) *t* = 0.2

(**c**) *t* = 0.4

(**d**) *t* = 0.6

(**e**) *t* = 0.8

(**f**) *t* = 1.0

**Figure 17.** Comparison of results with the exact solution.

## 5. Conclusions

This study proposed the TRPSF for solving convection–diffusion equations. The following findings were obtained:

This study presented a novel spatial and temporal discretization scheme for the convection–diffusion equation by using the proposed TRPSF. Because the TRPSF and its corresponding derivatives are smooth and nonsingular series functions, the shape parameter is not required for analysis.

In the proposed method, we transformed an initial value problem into an inverse boundary value problem. The problem could be solved in space–time coordinates by using the space–time initial and boundary conditions. Accordingly, the time-marching algorithm may not be required in the presented approach. The numerical solutions revealed that we could achieve more accurate numerical solutions than can the RBFCM using the time–marching scheme.

Highly accurate results could be obtained by adopting higher-order space–time radial polynomial terms using the presented TRPSF. The results indicate that the presented TRPSF is more accurate than is the RBFCM using different RBFs with optimal shape parameters for solving the convection–diffusion equation.

## References

1. Li, L.Y.; Jiang, Z.W.; Yin, Z. Fourth-order compact finite difference method for solving two-dimensional convection-diffusion equation. *Adv. Differ. Equ.* **2018**, *234*, 1–24. [CrossRef]
2. Cornejo, I.; Hayes, R.E.; Nikrityuk, P. A new approach for the modeling of turbulent flows in automotive catalytic converters. *Chem. Eng. Res. Des.* **2018**, *140*, 308–319. [CrossRef]
3. Ambrosetti, M.; Bracconi, M.; Maestri, M.; Groppi, G.; Tronconi, E. Packed foams for the intensification of catalytic processes: Assessment of packing efficiency and pressure drop using a combined experimental and numerical approach. *Chem. Eng. J.* **2020**, *382*, 122801. [CrossRef]
4. Appadu, A.R. Numerical solution of the 1D advection-diffusion equation using standard and nonstandard finite difference schemes. *J. Appl. Math.* **2013**, 1–14. [CrossRef]
5. Tony, W.H.; Sheu, C.F.; Chen, W.S. A novel two-dimensional convection-diffusion finite-difference scheme. *Numer. Heat Transf. B-Fundam.* **2000**, *38*, 369–387. [CrossRef]
6. Salkuyeh, D.K. On the finite difference approximation to the convection–diffusion equation. *Appl. Math. Comput.* **2000**, *179*, 79–86. [CrossRef]
7. Cornejo, I.; Cornejo, G.; Nikrityuk, P.; Hayes, R.E. Entry length convective heat transfer in a monolith: The effect of upstream turbulence. *Int. J. Therm. Sci.* **2019**, *138*, 235–246. [CrossRef]
8. Ramadhyani, S.; Patankar, S.V. Solution of the convection-diffusion equation by a finite-element method using quadrilateral elements. *Numer. Heat Transf. A-Appl.* **1985**, *8*, 595–612.
9. Cunha, C.L.N.; Carrer, J.A.M.; Oliveira, M.F.; Costa, V.L. A study concerning the solution of advection-diffusion problems by the boundary element method. *Eng. Anal. Bound. Elem.* **2016**, *65*, 79–94. [CrossRef]
10. Bertrand, F.; Devals, C.; Vidal, D.; Préva, C.S.D.; Hayes, R.E. Towards the simulation of the catalytic monolith converter using discrete channel-scale models. *Catal. Today.* **2012**, *188*, 80–86. [CrossRef]
11. Greiner, R.; Prill, T.; Van Setten, B.A.A.L.; Votsmeier, M. Tomography based simulation of reactive flow at the micro-scale: Particulate filters with wall integrated catalyst. *Chem. Eng. J.* **2020**, *378*, 121919. [CrossRef]
12. Li, B.Q.; Evans, J.W. Boundary element solution of heat convection-diffusion problems. *J. Comput. Phys.* **1991**, *93*, 255–272. [CrossRef]

13.  Sacco, R.; Stynes, M. Finite element methods for convection-diffusion problems using exponential splines on triangles. *Comput. Math. Appl.* **1998**, *35*, 35–45. [CrossRef]

14.  Suman, V.K.; Sengupta, T.K.; Jyothi Durga Prasad, C.; Surya Mohan, K.; Sanwalia, D. Spectral analysis of finite difference schemes for convection diffusion equation. *Comput. Fluids.* **2017**, *150*, 95–114. [CrossRef]

15.  Chen, W.; Fu, Z.J.; Chen, C.S. *Recent Advances in Radial Basis Function Collocation Methods*; Springer: Heidelberg/Berlin, Germany, 2014.

16.  Hardy, R.L. Multiquadric equations of topography and other irregular surfaces. *J. Geophys, Res.* **1971**, *176*, 1905–1915. [CrossRef]

17.  Kansa, E.J. Multiquadrics—A scattered data approximation scheme with applications to computational fluid-dynamics—I surface approximations and partial derivative estimates. *Comput. Math. Appl.* **1990**, *19*, 127–145. [CrossRef]

18.  Kansa, E.J. Multiquadrics—A scattered data approximation scheme with applications to computational fluid-dynamics—II solutions to parabolic, hyperbolic and elliptic partial differential equations. *Comput. Math. Appl.* **1990**, *19*, 147–161. [CrossRef]

19.  Xie, H.T.; Li, D.F. A meshless method for Burgers' equation using MQ-RBF and high-order temporal approximation. *Appl. Math. Model.* **2013**, *37*, 9215–9222. [CrossRef]

20.  Yang, J.Y.; Liu, X.F.; Wen, P.H. The local Kansa's method for solving Berger equation. *Eng. Anal. Bound. Elem.* **2015**, *57*, 16–22. [CrossRef]

21.  Li, M.; Jiang, T.S.; Hon, Y.C. A meshless method based on RBFs method for nonhomogeneous backward heat conduction problem. *Eng. Anal. Bound. Elem.* **2010**, *34*, 785–792. [CrossRef]

22.  Grabski, J.K.; Kołodziej, J.A. Laminar fluid flow and heat transfer in an internally corrugated tube by means of the method of fundamental solutions and radial basis functions. *Comput. Math. Appl.* **2018**, *75*, 1413–1433. [CrossRef]

23.  Qian, Z.; Hon, Y.C.; Xiong, X.T. Numerical solution of two-dimensional radially symmetric inverse heat conduction problem. *J. Inverse Ill-pose. P.* **2015**, *23*, 121–134. [CrossRef]

24.  Li, J.; Chen, Y.; Pepper, D. Radial basis function method for 1-D and 2-D groundwater contaminant transport modeling. *Comput. Mech.* **2003**, *32*, 10–15. [CrossRef]

25.  Bayona, V.; Moscoso, M.; Kindelan, M. Optimal constant shape parameter for multiquadric based RBF-FD method. *J. Comput. Phys.* **2011**, *230*, 7384–7399. [CrossRef]

26.  Golbabai, A.; Mohebianfar, E.; Rabiei, H. On the new variable shape parameter strategies for radial basis functions. *Comp. Appl. Math.* **2002**, *191*, 2611–2630. [CrossRef]

27.  Tsai, C.S.; Kolibal, J.; Li, M. The golden section search algorithm for finding a good shape parameter for meshless collocation methods. *Eng. Anal. Bound. Elem.* **2010**, *34*, 738–746. [CrossRef]

28.  Ng, Y.L.; Ng, K.C.; Sheu, T.W.H. A new higher-order RBF-FD scheme with optimal variable shape parameter for partial differential equation. *Numer. Heat Transf. B-Fundam.* **2019**, *75*, 289–311. [CrossRef]

29.  Espinoza, H.; Codina, R.; Badia, S. On some time marching schemes for the stabilized finite element approximation of the mixed wave equation. *Comput. Method Appl. M.* **2015**, *296*, 295–326. [CrossRef]

30.  Young, D.L.; Gu, M.H.; Fan, C.M. The time-marching method of fundamental solutions for wave equations. *Eng. Anal. Bound. Elem.* **2009**, *33*, 1411–1425. [CrossRef]

31.  Wang, H.J.; Shu, C.W.; Zhang, Q. Stability analysis and error estimates of local discontinuous Galerkin methods with implicit-explicit time-marching for nonlinear convection-diffusion problems. *Appl. Math. Comput.* **2016**, *272*, 237–258. [CrossRef]

32.  Yue, X.X.; Wang, F.J.; Hua, Q.S.; Qiu, X.Y. A novel space-time meshless method for nonhomogeneous convection-diffusion equations with variable coefficients. *Appl. Math. Lett.* **2019**, *92*, 144–150. [CrossRef]